Using an Isohaline Flux Analysis to Predict the Salt Content in an Unsteady Estuary

MATTHEW D. RAYSON

The Bob and Norma Street Environmental Fluid Mechanics Laboratory, Department of Civil and Environmental Engineering, Stanford University, Stanford, California, and School of Civil, Environmental, and Mining Engineering, and the Oceans Institute, University of Western Australia, Nedlands, Western Australia, Australia

EDWARD S. GROSS

The Bob and Norma Street Environmental Fluid Mechanics Laboratory, Department of Civil and Environmental Engineering, Stanford University, Stanford, and Center for Watershed Sciences, University of California, Davis, Davis, California

ROBERT D. HETLAND

Department of Oceanography, Texas A&M University, College Station, Texas

OLIVER B. FRINGER

The Bob and Norma Street Environmental Fluid Mechanics Laboratory, Department of Civil and Environmental Engineering, Stanford University, Stanford, California

(Manuscript received 3 June 2016, in final form 10 September 2017)

ABSTRACT

An estuary is classified as unsteady when the salinity adjustment time is longer than the forcing time scale. Predicting salt content or salt intrusion length using scaling arguments based on a steady-state relationship between flow and salinity is inaccurate in these systems. In this study, a time-dependent salinity box model based on an unsteady Knudsen balance is used to demonstrate the effects of river flow, inward total exchange flow (tidal plus steady), and the salinity difference between inflow and outflow on the salt balance. A key component of the box model is a relationship that links the normalized difference between inflowing and outflowing salinity at the mouth and the mean salinity content. The normalized salinity difference is shown to be proportional to the mean salinity squared, based on theoretical arguments from the literature. The box model is validated by hindcasting 5 years of mean salinity in Galveston Bay (estimated from coarse observations) in response to highly variable river discharge. It is shown that this estuary typically has a long adjustment time relative to the forcing time scales, and, therefore, the volume-averaged salinity rarely reaches equilibrium. The box model highlights the reasons why the adjustment time in a large, partially mixed estuary like Galveston Bay is slower when the mean salt content is higher. Furthermore, it elucidates why the salt content in the estuary is more responsive to changes in river flow than in landward exchange flow at the estuary mouth, even though the latter quantity is usually several times larger.

1. Introduction

Salinity is a key property for characterizing estuaries. There is extensive estuarine physics literature focused on mechanisms controlling the salt balance (see Geyer 2010; Geyer and MacCready 2014, and references therein). Low-inflow estuaries are defined as systems in which the evaporation exceeds freshwater runoff, or the freshwater discharge is sporadic (see, e.g., Largier 2010). These systems are rarely in steady state, and the unsteadiness term can have first-order effects on the salt balance (Banas et al. 2004).

Much of the theoretical understanding of estuarine circulation assumes the salinity distribution and forcing is in a steady state (Guha and Lawrence 2013; Geyer and MacCready 2014). An estuary is assumed to be steady (or quasi-steady) if the estuarine response time scale is shorter than the forcing time scale, which, for example, is the case for the Hudson River during high river flow

Corresponding author: Matthew D. Rayson, matt.rayson@uwa.edu.au

DOI: 10.1175/JPO-D-16-0134.1

(Chen et al. 2012). This response time scale is called the adjustment time T_{adj} and is formally the e-folding time of the salinity response to a small step change in forcing, such as river flow or tidal mixing (Kranenburg 1986; MacCready 1999, 2007). The adjustment time and the forcing time scale, therefore, determine whether one must consider unsteadiness when analyzing the salinity variability of a particular estuary.

MacCready (2007) derived a relationship between adjustment time and freshwater replacement time in a straight estuary subject to baroclinic exchange flow by

$$T_{adj} = \frac{1}{2}\frac{1}{\gamma}\frac{L}{\overline{u}}, \tag{1}$$

where L is the estuary length, $\overline{u}$ is the mean velocity due to river discharge, $L/\overline{u}$ is the freshwater replacement time, and the theoretical parameter $\gamma = 3$, based on a linearized salt balance for exchange-dominated systems. Lerczak et al. (2009) show that the response time is shorter ($\gamma = 4.5$) when stratification effects are included in the parameterization of exchange flow. Chen (2015) found that T_{adj} is actually a nonlinear function of the salt intrusion length L_x. The significance of this finding is twofold: the salinity in an estuary will change at a different rate during rising and falling river flows, and Eq. (1) is not strictly accurate for estuaries with large changes in river discharge. Monismith (2017) formalized this result into an integral model.

The salt intrusion length scale L_x is the horizontal distance of an isohaline from the estuary mouth. It has important implications for water quality and ecology. For example, in Galveston Bay, midsalinity water (10–15 psu) is considered optimal oyster habitat (Powell et al. 2003). In the San Francisco Estuary, the location of the 2-psu isohaline L_2 (referred to as X_2) is found to be correlated with an abundance of many pelagic species (Jassby et al. 1995). Length L_x is also useful in estimating the total salt mass in an estuary. Various estuaries exhibit self-similarity between the normalized salinity and the horizontal position normalized by L_x (e.g., Monismith et al. 2002; Lerczak et al. 2009). Self-similarity makes it possible to extrapolate the total volume-integrated salinity from L_x. It can therefore be used as an indicator of estuarine response to changes in forcing and to deduce relevant time scales. However, in geometrically complex systems, like many of the estuaries along the Gulf of Mexico and the U.S. East Coast, it can be difficult to obtain an unambiguous salt intrusion length; therefore, the volume-averaged salinity is a more suitable metric for total salt content.

Kranenburg (1986) and MacCready (2007) assume that the salt budget in an estuary is the sum of a steady response and a transient response. The adjustment time is then an averaging time scale to remove the transients and retain the steady-state dynamics. However, this assumption is questionable in highly unsteady systems, such as Willapa Bay, Washington (Banas et al. 2004), where several order of magnitude variations in river flow, or tidal forcing, occur at time scales that are short relative to the adjustment time.

The main purpose of this paper is to develop a simple model that captures salinity evolution in an unsteady estuary and to then use the model to demonstrate how adjustment time varies based on the estuarine state, namely, the mean salinity. The box model uses the variables associated with the total exchange flow as its inputs. Galveston Bay is used as a case study because, as we will demonstrate, the exchange flow is due to a combination of tidal and subtidal processes; it has irregular geometry (meaning the salt intrusion length is difficult to unambiguously define); and it is unsteady, in that the adjustment time is longer than the forcing time scale. Galveston Bay has similar physical characteristics to many other Gulf of Mexico and U.S. East Coast estuaries—for example, Mobile Bay and Pamlico Sound—in that they have a barrier island–type morphology, and freshwater inputs are intermittent (see, e.g., Orlando 1993). We therefore expect the model presented here to be readily applicable to this class of low-inflow estuaries.

We begin with a brief review of the estuarine salt balance and total exchange flow concept, and then present a solution to an unsteady Knudsen relationship that characterizes the important processes and time scales. An analysis of the salinity variability of a three-dimensional (3D) numerical model that captures the response of Galveston Bay to transient river forcing is then conducted to determine the total exchange flow terms in the estuary and how they vary as a function of forcing and mean salinity. Total exchange flow variables are either calculated directly from the 3D model or determined by empirically fitting box-model parameters to match salinity predictions during a 6-month 3D model simulation period and then to hindcast a longer 5-yr period when there were adequate observations available for validation but no numerical model data. Last, we examine the dependence of the adjustment time scale on river discharge, exchange flow at the mouth, normalized salinity difference at the mouth, and volume-averaged salinity. The adjustment time is used to compare Galveston Bay with other estuaries.

2. Total exchange flow and the mean salt balance

MacCready (2011) defines the cross-sectional flux in isohaline coordinates, that is, $Q = Q(s, x, t)$:

$$Q(s,x,t) = \left\langle \int_{A_s} u\, dA \right\rangle, \tag{2}$$

where A_s is the cross-sectional area with salinity greater than s at an along-estuary cross section with coordinate x, and angle brackets denote a tidal average (filter). The sign convention used here is $Q > 0$ represents landward flow, while $Q < 0$ is seaward flow. The advantage of representing the transport in isohaline (isopycnal) coordinates is that the inflow and outflow are categorized based on their salinity class, with the overall goal of separating inflowing ocean water from outflowing, mixed-estuarine water. MacCready (2011) termed the isohaline flux in Eq. (2) as the total exchange flow (TEF) because it captures both tidal (e.g., tidal pumping) and subtidal (e.g., baroclinic circulation) exchange processes.

The TEF technique exactly satisfies an unsteady Knudsen relationship (Knudsen 1900),

$$\begin{aligned}\frac{d}{dt}(\bar{\bar{s}}V) &= Q_{\text{in}}s_{\text{in}} + Q_{\text{out}}s_{\text{out}} \\ &= F_{\text{in}}(x=0) + F_{\text{out}}(x=0),\end{aligned} \tag{3}$$

where $\bar{\bar{s}} = \int s\, dV/V$ is the volume-averaged salinity, and V is the tidally averaged volume that is defined so that there is no salt transport on the landward end. In practice, we assume this equal to the total physical volume of the estuary. Terms in the salt balance [Eq. (3)] are derived from the isohaline-decomposed flux; the inward and outward salt transport is given by

$$F_{\text{in}} = \int_0^{s_o} s\frac{\partial Q}{\partial s}\bigg|_{\text{in}} ds, \quad \text{and} \tag{4}$$

$$F_{\text{out}} = \int_0^{s_o} s\frac{\partial Q}{\partial s}\bigg|_{\text{out}} ds, \tag{5}$$

where s_o is the ocean salinity value. The inward and outward TEF terms are given by

$$Q_{\text{in}} = \int_0^{s_o} \frac{\partial Q}{\partial s}\bigg|_{\text{in}} ds, \quad \text{and} \tag{6}$$

$$Q_{\text{out}} = \int_0^{s_o} \frac{\partial Q}{\partial s}\bigg|_{\text{out}} ds, \tag{7}$$

so that the average incoming and outgoing salinity are defined by

$$s_{\text{in}} = \frac{F_{\text{in}}}{Q_{\text{in}}}, \quad \text{and} \tag{8}$$

$$s_{\text{out}} = \frac{F_{\text{out}}}{Q_{\text{out}}}. \tag{9}$$

In practice, the fluxes were estimated by evaluating Eq. (2) with binned salinities, and a Godin filter was used to average over a subtidal time scale. As previously mentioned, the exchange flow in Eq. (2) has been termed the total exchange flow by MacCready (2011), as it includes contributions from both tidal and subtidal processes, that is,

$$Q(s) = Q_{\text{Eu}}(s) + Q_T(s), \tag{10}$$

where $Q_T(s)$ represents all residual tidal flux terms (e.g., tidal pumping and trapping), and $Q_{\text{Eu}}(s)$ is the subtidal or Eulerian residual flux. Following Chen et al. (2012), the Eulerian flux is given by

$$Q_{\text{Eu}}(s) = \int_{A_s^{\text{Eu}}} \langle u\rangle\langle dA\rangle, \tag{11}$$

where A_s^{Eu} is the cross-sectional area with subtidal salinity greater than s, and $\langle u\rangle$ is the subtidal velocity. This exchange flow can be generated by a number of physical mechanisms including baroclinic (gravitational) circulation, strain-induced periodic stratification (Simpson et al. 1990), and tidal asymmetry in lateral circulation (Lerczak and Geyer 2004).

a. An unsteady salt balance model

A box model of salt mass elucidates the important variables required to understand estuarine response because of variations in forcing. We start out with the unsteady Knudsen relationship [from Eq. (3)]:

$$V\frac{d\bar{\bar{s}}}{dt} + \bar{\bar{s}}\frac{dV}{dt} = Q_{\text{in}}s_{\text{in}} + Q_{\text{out}}s_{\text{out}}, \tag{12}$$

and conservation of volume,

$$\frac{dV}{dt} = Q_{\text{in}} + Q_{\text{out}} + Q_r, \tag{13}$$

where dV/dt is the subtidal volume change due to barotropic fluxes, and Q_r is the river discharge. Defining the normalized mean salt content $\Sigma = \bar{\bar{s}}/s_{\text{in}}(x=0)$ and the normalized salinity difference $\delta = (s_{\text{in}} - s_{\text{out}})/s_{\text{in}}$, Eqs. (12) and (13) are combined to give

$$\frac{d\Sigma}{dt} = \frac{Q_{\text{in}}}{V}\delta - \frac{Q_r}{V}(1-\delta) + \frac{1-(\delta+\Sigma)}{V}\frac{dV}{dt}. \tag{14}$$

Here, we have assumed that ds_{in}/dt is small, relative to $d\bar{s}/dt$, and can be ignored from the left-hand side. Equation (14) states that the time-rate of change of normalized salinity is balanced by the inward TEF, river discharge, and barotropic fluxes. Note that in an estuary dominated by gravitation circulation, the normalized salinity difference δ is equivalent to the normalized stratification, although this is not true when tidal processes like tidal pumping dominate exchange. The normalized salinity difference influences the relative contribution of each flux term Q_{in} and Q_r. Assuming that river discharge, water level, and ocean salinity are known (or measured) for a given estuary, one must then either measure or model Q_{in} and δ to predict the mean salinity.

Geyer (2010) shows that δ can be predicted using a freshwater Froude number according to

$$\delta = c_1 \mathrm{Fr}_f^{2/3}, \tag{15}$$

where $\Delta s = s_{in} - s_{out}$, Fr_f is given by

$$\mathrm{Fr}_f = \frac{Q_r}{A\sqrt{g'H}}, \tag{16}$$

c_1 is an empirical constant [Geyer (2010) found $c_1 = 3.4$ based on an empirical fit to many estuaries], g' is the reduced gravity taken from the density difference between fresh and ocean water, A is the cross-sectional area, and H is the depth. Guha and Lawrence (2013) show that

$$\delta = C_1 \mathrm{Fr}_f^{2/3} (\overline{\Sigma}_{X,0})^2 + C_2 \mathrm{Fr}_f^{4/3} (\overline{\Sigma}_{X,0}), \tag{17}$$

where $C_1 = 7.06$, $C_2 = 8.82$, and $\overline{\Sigma}_{X,0}$ is the longitudinal salinity gradient at the mouth. Guha and Lawrence (2013) argue that a second parameter, a tidal Froude number, is also necessary to predict the longitudinal salinity gradient under steady-state conditions (not shown here). The Froude number dependence arises from nondimensionalizing the estuarine salt balance equations with the internal wave phase speed (see MacCready 1999). Empirical coefficients in Eq. (17) arise from assumptions about the estuary geometry, exchange-flow scaling, and vertical mixing. Note that both Geyer (2010) and Guha and Lawrence (2013) δmodels rely on a steady-state assumption and, hence, constant Fr_f.

So long as δ is a nonlinear function of Σ, as in Eq. (17), the only other unknown variable is the inward total exchange flow Q_{in}. The goal of this paper is to determine a $\delta - \Sigma$ relationship and calculate Q_{in} directly using the TEF decomposition applied to a validated 3D numerical model of a realistic, unsteady estuary. We will then show how the TEF terms relate back to empirical forms of the steady and tidal exchange rates (see, e.g., MacCready 2004; Banas et al. 2004; Ralston et al. 2008).

b. Adjustment time

Adjustment time can be expressed as the inverse of the rate of change of salinity

$$\tau_{adj} = \frac{\Sigma}{|d\Sigma/dt|}. \tag{18}$$

Using Eq. (14) and assuming $\delta + \Sigma \approx 1$ (i.e., $s_{out} \approx \bar{s}$) so we can ignore the volume tendency term (we will also show later that its contribution is negligible) results in

$$\tau_{adj} = \frac{V\Sigma}{|Q_{in}\delta - Q_r(1-\delta)|}. \tag{19}$$

Equation (19) shows that there are two time scales of interest, namely, the ocean water replacement time $V/(Q_{in}\delta)$ and the freshwater replacement time $V/[Q_r(1-\delta)]$. It also shows the role of the normalized salinity difference in linking the two fluxes to the estuarine adjustment. Salt mass will increase when $Q_{in}\delta > Q_r(1-\delta)$ and decrease when the opposite is true. Steady state is reached if $Q_{in}\delta = Q_r(1-\delta)$. The adjustment time goes to infinity in this case and has no relevant meaning, as the system has indeed adjusted.

Normalizing the hydraulic residence time (or freshwater replacement time) $\tau_h = V/Q_r$ by the adjustment time gives the estuarine speedup factor τ^* (e.g., Hetland and Geyer 2004):

$$\tau^* = \frac{\tau_h}{\tau_{adj}} = \frac{Q_{in}}{Q_r}\frac{\delta}{\Sigma} - \frac{1-\delta}{\Sigma}. \tag{20}$$

The estuarine speedup factor indicates how much faster an estuary will respond than the freshwater replacement time. Equation (20) shows that for any estuary, τ^* depends on three variables, namely, the normalized volume-averaged salinity Σ, the normalized salinity difference at the mouth δ, and the ratio of inward exchange flow to river flow Q_{in}/Q_r. Assuming a $\delta - \Sigma$ relationship like Eq. (17) and inserting it into Eq. (20) demonstrates how nonlinearities arise in the speedup factor (or the adjustment time).

3. Total exchange flow in Galveston Bay

a. Study site

The study site is Galveston Bay, Texas, a wide and shallow (3 m) estuary with a 15-m deep, narrow, shipping channel running along its length. The bay is microtidal

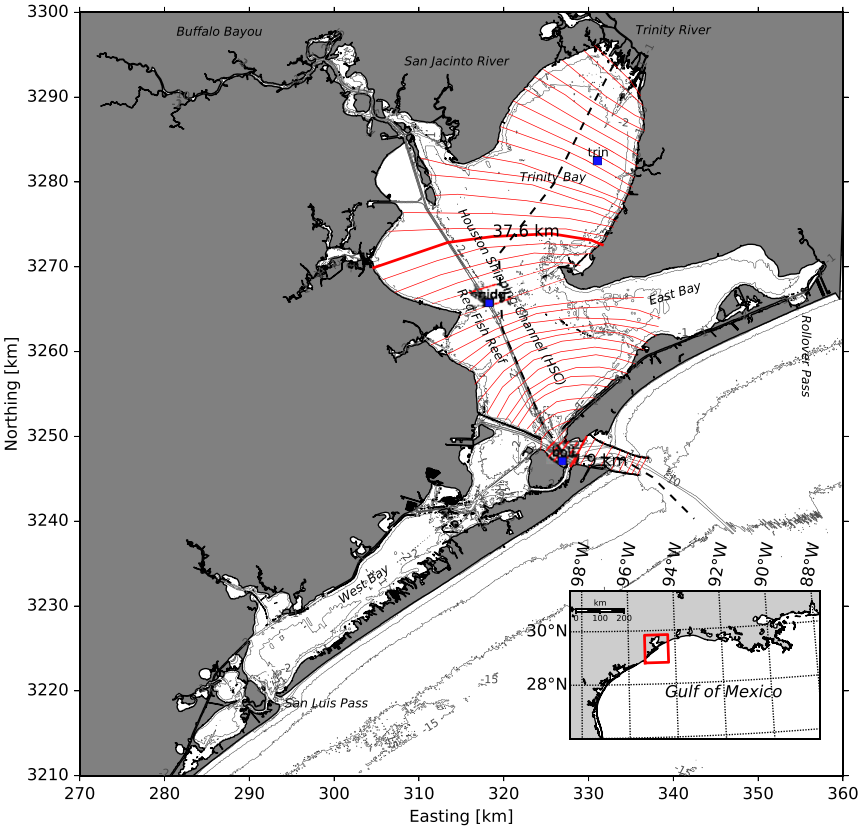

FIG. 1. Location of the center axis (dashed black) and the series of transects (red) that form the along- and across-estuary coordinates for Galveston Bay. The blue dots indicate salinity monitoring stations.

(<0.5 m), although the tidal currents through the main entrance exceed 1.0 m s^{-1} (Rayson et al. 2015). Typical annual peak river discharge of 1000–3000 m^3 s^{-1} occurs intermittently and is generally preceded by several months of low $\sim O(10)$ m^3 s^{-1} discharge. There is, however, significant interannual variability in the river discharge. In addition to variability in river flow, salinity at the inlet is variable because the circulation on the Texas–Louisiana shelf intermittently drives lower-salinity water (~24 psu) past the mouth of Galveston Bay. Subtidal water-level fluctuations driven by wind stress and barometric effects also drive flow through the mouth of the estuary and, thereby, contribute to the variability of salinity within the estuary (Rayson et al. 2015).

The complex geometry of Galveston Bay makes it difficult to define a dominant along-estuary axis (Fig. 1). The main thalweg, the Houston Shipping Channel (HSC), does not connect to the main freshwater source, the Trinity River. As our main concern is the mixing of freshwater through the estuary, we define a center line for the main axis running from the Trinity River through Trinity Bay before meeting the HSC at Red Fish Reef, and finally following the HSC out of the mouth (Fig. 1). We then used GIS software to draw a series of 50 transects that run approximately perpendicular to this center line and define the lateral coordinate as the distance along the transect from center line. Note that West Bay and East Bay have not been included in these transects because they form side arms of the main estuary.

b. 3D numerical model description

We applied the 3D Stanford Unstructured Nonhydrostatic Terrain-following Adaptive Navier-Stokes Simulator (SUNTANS) hydrodynamic model (Fringer et al. 2006) to hindcast salinity over a 6-month period between March and September 2009. SUNTANS solves the 3D Reynolds-averaged Navier–Stokes equations discretized on an unstructured horizontal grid. We have used the same model setup as described in Rayson et al. (2015, 2016), in particular the mixed quadrilateral–triangular grid configuration. This grid consists of 57 305 horizontal grid cells with a median resolution of 100 m in the shipping channel and estuary mouth regions. Twenty fixed z-layers discretized the vertical coordinate. Tidal boundary conditions were prescribed using a blend of gauge data and a Gulf of Mexico regional tidal model that provided spatial

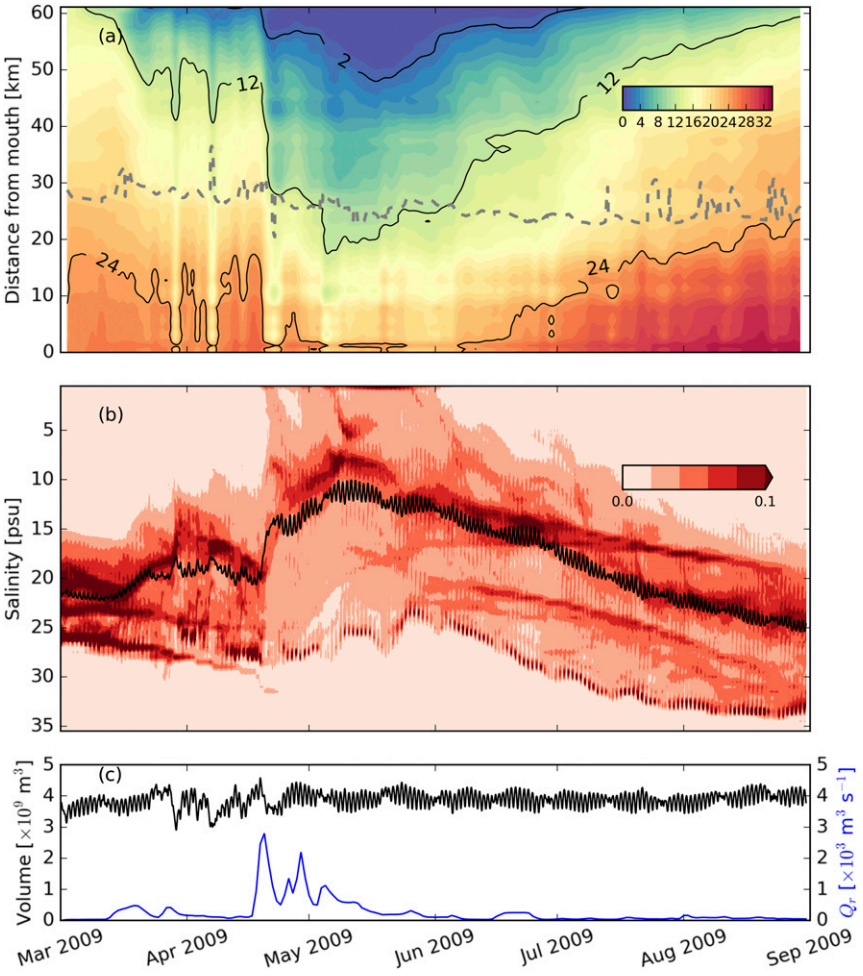

FIG. 2. (a) Time series of the laterally averaged salinity as a function of distance along the estuarine channel. The gray dashed line shows the distance along axis to the volumetric mean salinity (L_s). (b) Volume-weighted PDF of salinity with the mean ($\overline{s}$) represented by the solid black line. (c) Total volume inside of the estuary (black) and river discharge (blue) over the corresponding time period. The black contours in (a) indicate the 2-, 12-, and 24-psu isohalines. Note that the salinity scale in (b) is inverted to represent ocean water at the bottom and freshwater at the top to be consistent with (a).

tidal amplitude and phase information; temperature and salinity data were interpolated from a shelf-scale ROMS model configuration (Marta-Almeida et al. 2013). Realistic river discharge and atmospheric heat, salt, and momentum fluxes were also prescribed. The model resolved the shipping channel and accurately represented long-term salt intrusion, thus making it suitable for studying the salinity dynamics. See Rayson et al. (2015) for details of the model validation against observations of long-term salinity, water level, temperature, and currents.

c. *Salinity variability*

The time evolution of the laterally averaged salinity is shown in Fig. 2a. Locations of individual isohalines can be inferred directly from Fig. 2a; the 2-, 12-, and 24-psu isohalines (L_2, L_{12}, L_{24}) are represented by the black contours. The volume-weighted probability density function (PDF) of salinity was calculated at each model time step by calculating a histogram of salinity in 0.5-psu bins and is shown in Fig. 2b. River discharge and total volume over the same corresponding time period are shown in Fig. 2c. The total volume of water in each salinity class can be computed directly by multiplying the PDF by the total volume.

The largest freshwater excursion, and, hence, drop in mean salinity, occurred following the high-discharge event between mid-April and mid-May, when the average $Q_r = 1100\,\mathrm{m^3\,s^{-1}}$. There was a lag in the salinity

drop following the flooding event; peak discharge occurred around 20 April (Fig. 2c), while the minimum mean salinity occurred around 10 May 2009 (Fig. 2b). In addition to this lag, individual peaks in river discharge on time scales of 3–10 days did not manifest in the mean salinity. This salinity response shows how the estuary acts as a lagged filter for the river flow and demonstrates that the time history of the flow, not just the instantaneous river flow, influences the low-frequency response. Following June, there were no discharge events with $Q_r > 1000\,\mathrm{m^3\,s^{-1}}$, and the average discharge dropped to $125\,\mathrm{m^3\,s^{-1}}$, allowing the mean salinity to increase at an approximately constant rate.

As shown in Fig. 2, several 20–30-km excursions of the 12-psu isohaline with periods of 3–10 days occurred at the end of March and in early April. These perturbations coincided with strong, low-pressure storms that caused water-level oscillations with the same period and subsequently drove subtidal barotropic flows through the entrance of the bay. Large-surface stress, driven by the mainly northerly winds, was also a consequence of these storms. The overall effect on the mean salinity (Fig. 2b) was weak, however; the mean salinity decreased by 2–3 psu and quickly recovered poststorm.

The salinity PDF indicates the distribution of different water masses over time within Galveston Bay. Two main peaks were present in the PDF (Fig. 2b) for a majority of the time: a Gulf salinity peak (25–35 psu) and a midsalinity peak (10–25 psu). A third peak spanning 0–10 psu was also present between April and July representing the water mass discharged from the river. The location of the midsalinity peak was roughly aligned with the mean; it dropped during high river flow and gradually increased from June 2009 onward. During this period of salinity increase, the midsalinity water volume increased at roughly the same rate as the Gulf salinity peak, with the Gulf peak roughly 50% higher than the midsalinity value.

The estuarine adjustment time for the high- and low-discharge periods was 7 and 60 days, respectively; this was based on Eq. (1), (assuming $\overline{u}/L \equiv Q_r/V$) using the average flow rates (Q_r = 125 and $1100\,\mathrm{m^3\,s^{-1}}$, respectively), a constant volume ($V = 3.75 \times 10^9\,\mathrm{m^3}$), and $\gamma = 3$. Using the definition from Eq. (18) and the mean salinity from Fig. 2b, the adjustment time was, on average, 40 days during the high river-discharge period and 140 days during the low-discharge period. This discrepancy between the adjustment time predicted by Eq. (1) and the actual adjustment time given by Eq. (18) is likely to result from violating the underlying assumptions that the estuary is responding to a small step change in forcing and that gravitational circulation is the main driver of salt exchange (cf. Kranenburg 1986; MacCready 1999). This was not the case here: the river discharge changed by at least an order of magnitude (see Fig. 10c), and, as we will later demonstrate later, the exchange is tidally forced. The adjustment time predicted by Eq. (1) was therefore too fast for this estuary.

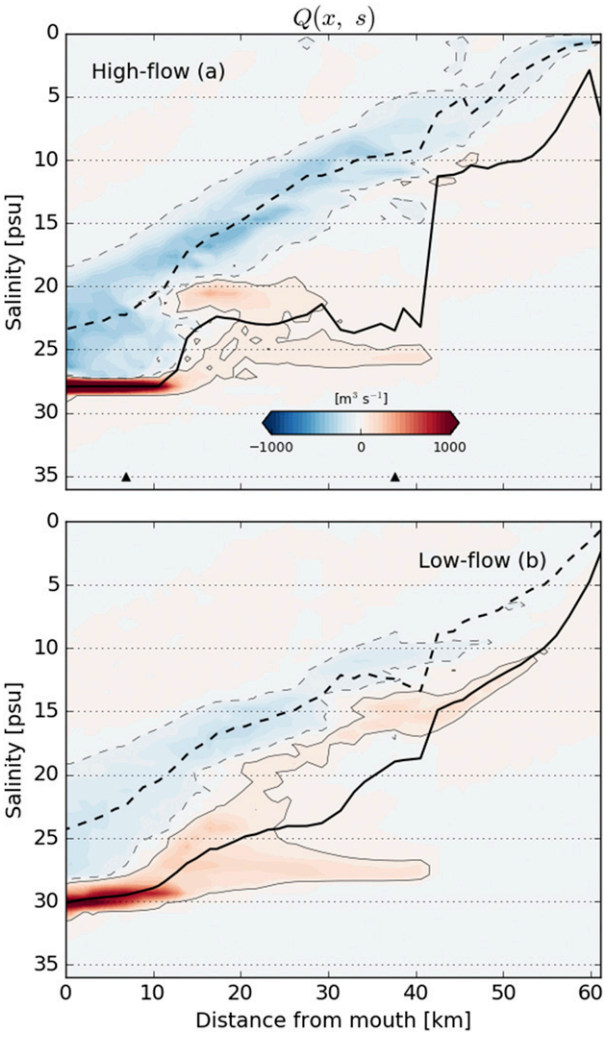

FIG. 3. Time-averaged discharge in salinity–distance space during (a) high-flow $Q(s, x, t$ = 2009/04/30) and (b) low-flow $Q(s, x, t$ = 2009/07/01) conditions. The thick solid and dashed black lines indicate s_{in} and s_{out}, respectively. The thin solid and dashed gray lines indicate the $\pm 50\,\mathrm{m^3\,s^{-1}}$ flow contours.

d. *Isohaline flux analysis*

Results of the isohaline flux decomposition [Eq. (2)] are shown in Figs. 3 and 4, which represent different 2D views of a 3D function $Q(s, x, t)$. In a 2D plane, we show both a time snapshot over the length of the estuary (Fig. 3) and the time variability at a cross section (Fig. 4). The locations of the two cross sections are shown in Fig. 1. Flow contours crossing a density surface (horizontal line

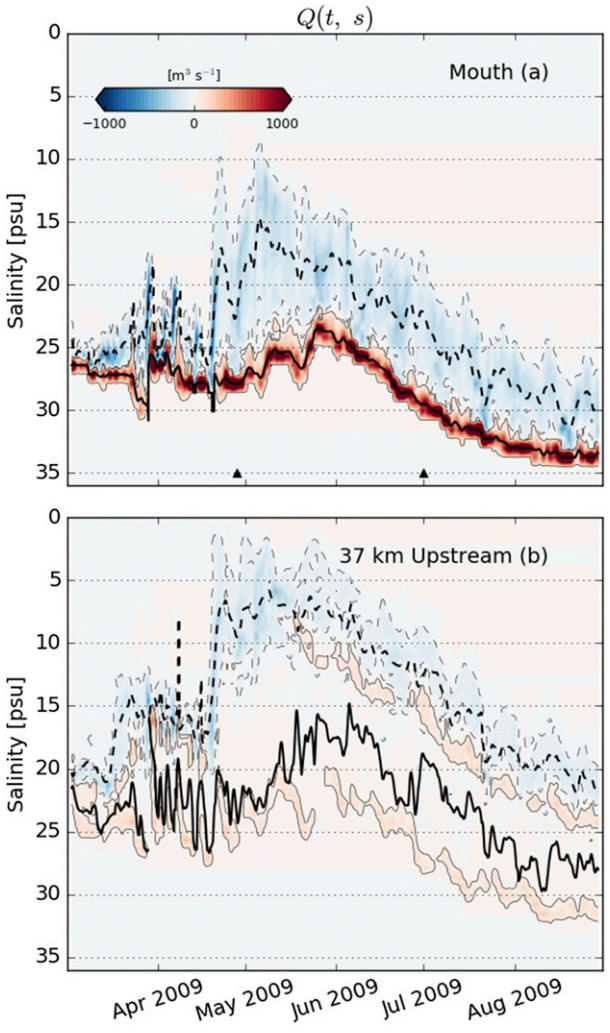

FIG. 4. Time-averaged discharge in salinity–time space at the (a) estuary mouth $Q(s, x = 7\,\text{km}, t)$ and (b) 37 km upstream $Q(s, x = 37\,\text{km}, t)$. The thick solid and dashed black lines indicate s_{in} and s_{out}, respectively. The thin solid and dashed gray lines indicate the $\pm 50\,\text{m}^3\,\text{s}^{-1}$ flow contours.

in this coordinate framework) indicate the diapycnal flux, or water mass transformation, caused by mixing.

Figure 3a shows the total exchange flow in isohaline coordinates during high-discharge conditions (1 May 2009). The outflow $[Q(s) < 0]$ starts at 0 psu near the river source and gradually transitions to a range of 18–27 psu at the estuary mouth. The inflow near the estuary mouth [indicated by contours of $Q(s) > 0$] was largely confined to 27 psu and gradually transitioned to 25 psu at $x = 25$ km. The up-estuary extent of $Q(s) > 50\,\text{m}^3\,\text{s}^{-1}$, shown by a gray contour in Fig. 3, extended to around $x = 40$ km during this high-discharge period.

In contrast to the high-discharge period, Fig. 3b shows the circulation during a period of net salt gain (1 July 2009). During this period, there was weak outflow near the river, and the inflow from the Gulf extended up to 53 km from the estuary mouth. The inflow formed two branches at around $x = 25$ km: one confined to about 28 psu and extending to 40 km up-estuary; the other branch transformed from 28 to 10 psu and intruded to 53 km up-estuary. We hypothesize that the two branches are different transport pathways for incoming Gulf water into the estuary. The first branch represents a high-salinity water tongue that intrudes along the shipping channel and does not mix appreciably with the estuary water. The second branch represents high-salinity water in the shallow regions that is transported up-estuary. Note that the cross sections diverge from the channel at $x = 40$ km (see Fig. 1); this can be seen in the cutoff of landward salt intrusion in Fig. 3.

The time evolution of the isopycnal flux at the mouth is shown in Fig. 4a. The landward flow $[Q(s) > 0]$ was confined to a narrow salinity band that generally followed the (time variable) Gulf salinity. The increase in inflow salinity from June to September corresponded with the evolving salinity on the Texas–Louisiana shelf. The outflow salinity covered a wider band that varied with river flow. The width of the band was greatest (10–25 psu) following the high-discharge period during April and May. Figure 4b shows the time evolution of the isohaline flux further upstream at $x = 37$ km, at a cross section shown by a thick red line in Fig. 1. Two separate inflow branches of high-salinity water are readily apparent in Fig. 4b, and both were modulated at a fortnightly time scale. These branches represent the high-salinity inflow in the shipping channel and the low-salinity inflow on the shoals that can be seen in the along-channel view of $Q(s)$ (Fig. 3).

The inflowing and outflowing salinities s_{in} and s_{out} [Eq. (9)] elucidate the transformation (mixing) of river and Gulf water in the estuary and their direction of flow. At the mouth, $s_{\text{in}}(x = 0)$ (Fig. 4a), roughly corresponds to the high-salinity peak in the PDF shown in Fig. 2b. The difference between the inflowing and outflowing salinity $\Delta s = s_{\text{in}}(x = 0) - s_{\text{out}}(x = 0)$ at the mouth varied between 2 and 10 psu, with a greater difference following high river flow. The outflowing salinity $s_{\text{out}}(x)$ increased linearly moving toward the mouth from 0 to 25 psu during both high- and low-flow conditions (Figs. 3a and 3b, respectively). During high flow, $s_{\text{in}}(x)$ was approximately 28 psu between 0 and 10 km and approximately 24 psu between 10 and 35 km. A sharp gradient in $s_{\text{in}}(x)$ was present roughly 35 km from the mouth during high flow, in the same region that the cross sections (shown in Fig. 1) diverged from the HSC.

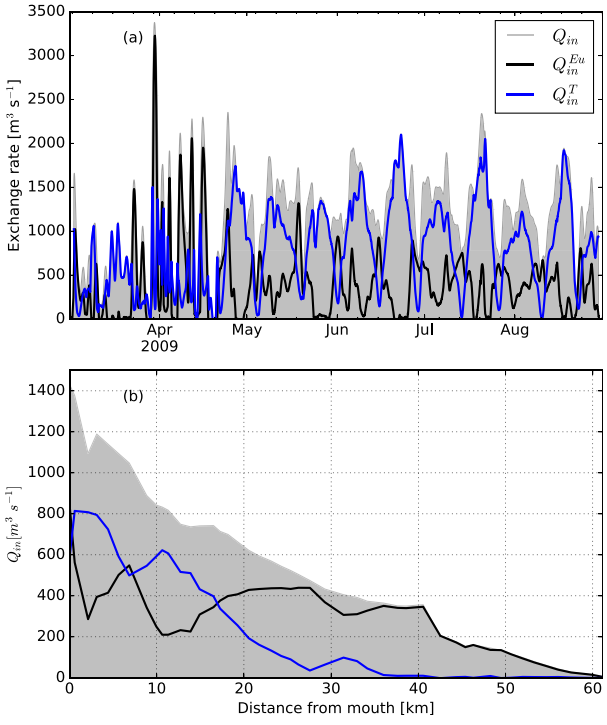

FIG. 5. (a) Total exchange flow at the mouth of Galveston Bay with the decomposed tidal and subtidal contributions superimposed, and (b) time-averaged and along-estuary Q_{in} and its components.

e. *Flux decomposition*

The TEF was decomposed into Eulerian residual and residual tidal fluxes using Eqs. (10) and (11) to further elucidate the exchange mechanisms. Figure 5a shows a time series of the two components across the mouth of Galveston Bay. Flow Q_{in} oscillated at a roughly 3-day period during April 2009 and then over a 14-day period thereafter. The residual tidal flux $Q_{\text{in}}^{T}(s)$ was the dominant component from May onward and was greatest during spring tides. The Eulerian flux $Q_{\text{in}}^{\text{Eu}}(s)$ also modulated with tidal forcing, although it peaked during neap tides. This suggests the steady exchange flow was strengthened by weaker vertical mixing during neap tides (e.g., Stacey et al. 2001). During storm periods, when barotropic fluxes associated with low-frequency water-level variations in the Gulf were large, $Q_{\text{in}}^{\text{Eu}}$ was also largest. On average, however, the tidal flux contributed roughly two-thirds of the total flux at the entrance. Following Hansen and Rattray (1966), this implies a diffusive fraction parameter $\nu = Q_{\text{in}}^{T}/Q_{\text{in}} = 0.66$ in Galveston Bay. The main consequence of this result is that tidal contributions to the salt flux, as well as the steady exchange, are necessary for a salt transport model in Gulf estuaries.

Along-estuary variations of the time-averaged TEF over the entire 6-month period are shown in Fig. 5b. Flow $Q_{\text{in}}(s)$ peaked at 1400 m^3 s^{-1} near the mouth of the estuary and decayed exponentially toward the river with an *e*-folding distance of roughly 35 km from the mouth. The tidal exchange term Q_{in}^{T}, representing exchange flow associated with tidal dispersion, decayed more rapidly with an *e*-folding distance 20 km from the mouth, and it vanished 45 km from the mouth, in Trinity Bay. The Eulerian flux term fluctuated between 800 and 200 m^3 s^{-1} and was roughly equal to the tidal exchange term up to 20 km from the mouth. It became the dominant term, contributing to more than 95% of the TEF greater than 20 km from the mouth. The implication is that even though tidal fluxes dominate at the mouth, salt transport is mainly driven by steady exchange flow upestuary, away from the mouth. Dronkers and Van de Kreeke (1986) refer to the tidal flux component as the "nonlocal" flux. They state that it is usually large in regions where the tidal velocity and salinity vary rapidly over distances proportional to one tidal excursion length, as is true for the mouth of Galveston Bay. The contribution of this tidal flux is also likely to be important at the mouth of other Gulf of Mexico estuaries where a narrow contraction opens into a wide, shallow interior.

4. Relationships between the TEF terms and the mean salinity

a. *Stratification model*

The nondimensional stratification δ at the mouth varied between 0.05 and 0.4 as shown in Fig. 6. Based on these results, Galveston Bay varied between partially mixed ($\delta > 0.1$) and well-mixed ($\delta < 0.1$) based on the definitions in Hansen and Rattray (1966). Note that the normalized salinity difference is derived from the tidally averaged TEF definition, not an instantaneous value. This result is in contradiction to the assumption that Gulf of Mexico estuaries are typically well-mixed, barotropic systems (see e.g., Officer 1976).

We model δ using Eq. (17) by assuming that the horizontal salinity gradient is linear, thus $\overline{\Sigma}_{X,0} = 1 - \Sigma$. The predicted stratification is also shown in Fig. 6, which was calculated using the mean river discharge as a representative value so that the freshwater Froude number $\text{Fr}_f = 0.06$. The gray-shaded region in Fig. 6 highlights the sensitivity of Eq. (17) to the Froude number. In general, Eq. (17) overpredicts the stratification, which is unsurprising given the simplifying assumptions used in its derivation and the choice of Froude number. A more practical model for the Galveston Bay data is to drop

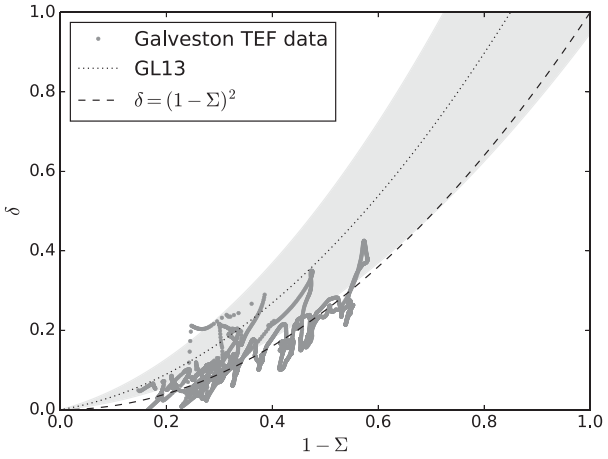

FIG. 6. Normalized stratification at the mouth δ plotted against the longitudinal salinity gradient $1 - \Sigma$ (see text). The dotted line shows the solution of Guha and Lawrence (2013) [GL13, Eq. (17)] with $\mathrm{Fr}_f = 0.06$, and the gray-shaded regions show possible solutions for $0.04 < \mathrm{Fr}_f < 0.1$. Equation (21) is indicated by the dashed line.

the second term in Eq. (17), since $C_2\mathrm{Fr}_f^{4/3} \approx 0.1$ and $C_1\mathrm{Fr}_f^{2/3} \approx 1$, resulting in

$$\delta = (1-\Sigma)^2. \tag{21}$$

This provides a better fit to the data in Fig. 6 and is physically justified. Furthermore, the relationship has the properties in the no-flow limit that $\delta = 0$ when $\Sigma = 1$ and those in the high-flow limit that $\delta = 1$ when $\Sigma = 0$, that is, $s_{\mathrm{out}} = 0$.

b. *Empirical relationships between Q_{in} and forcing*

To use the salinity box model [Eq. (14)] as a predictive tool, we empirically investigated the relationship between the inward total exchange flow Q_{in} and the estuarine forcing conditions at the mouth of Galveston Bay using the numerical model data. Similar to Chen et al. (2012), we compared the inward flux to three quantities, namely, the subtidal barotropic flux Q_η, the RMS tidal flux at the mouth Q_{rms}, and the gravitational exchange flux Q_g. The subtidal flux is due to subtidal water-level fluctuations and is given by (e.g., Wong and Moses-Hall 1998; Ralston et al. 2008)

$$Q_\eta = a_\eta A_{\mathrm{bay}} \frac{\partial\langle\eta\rangle}{\partial t} = a_\eta \frac{dV}{dt}, \tag{22}$$

where a_η is an empirical coefficient, A_{bay} is the surface area of the bay ($1.3 \times 10^9\,\mathrm{m}^2$), and $\partial\langle\eta\rangle/\partial t$ is the time-rate of change of subtidal water level at the mouth . Note that since we are only concerned with the inward flux, we set $Q_\eta = 0$ when $Q_\eta < 0$.

The RMS tidal flux Q_{rms} was computed by taking the total volume flux from the model through a cross section at the estuary mouth, removing the subtidal component using a Godin filter, and then using a 30-h sliding root-mean-square of the filtered volume flux. The gravitational exchange Q_g was estimated with (cf. Stacey et al. 2001; Monismith et al. 2002)

$$Q_g = a_g A_{\mathrm{mouth}} \frac{\beta g (d\langle s\rangle/dx) H^2}{u_*}, \tag{23}$$

where a_g is an undetermined empirical coefficient, β is the haline contraction coefficient, $d\langle s\rangle/dx$ is the subtidal estuarine salinity gradient, H is the water depth, A_{mouth} is the cross-sectional area at the mouth ($9660\,\mathrm{m}^2$), and u_* is the tidal friction velocity. The salinity gradient was calculated from the model by taking the difference in subtidal salinity at two sections close to the mouth, and the friction velocity was calculated with $u_* = \sqrt{C_d}(Q_{\mathrm{rms}}/A_{\mathrm{mouth}})$, where the drag coefficient $C_d = 2.5 \times 10^{-3}$.

Time series of the different flux scales and Q_{in} are shown in Fig. 7, and regression values against the different TEF terms are presented in Table 1. Table 1 shows that Q_η was most strongly correlated with $Q_{\mathrm{in}}^{\mathrm{Eu}}$ ($r^2 = 0.71$), and Q_{rms} was most strongly correlated with Q_{in}^{T} ($r^2 = 0.66$). Flow Q_g was weakly correlated with both Q_{in}^{T} and $Q_{\mathrm{in}}^{\mathrm{Eu}}$ ($r^2 = 0.11$ and 0.04, respectively). A 30-day rolling (or windowed) regression was calculated between each flux component and Q_{in} to show the time variability of the relationship (Fig. 7e). The correlation between the tidal flux Q_{rms} (Fig. 7b) and Q_{in}^{T} was high ($r^2 > 0.90$) between July and September (Fig. 7e), when river discharge was low and there were no significant storms. During April 2009, when several storm systems passed by, the correlation with the tidal flux was low ($r^2 < 0.5$). The correlation between $Q_{\mathrm{in}}^{\mathrm{Eu}}$ and the subtidal barotropic flux Q_η was best following this storm period ($r^2 \approx 0.95$). From June onward, the Eulerian flux $Q_{\mathrm{in}}^{\mathrm{Eu}}$ was correlated ($0.3 < r^2 < 0.5$) with the baroclinic flux (Q_g, Fig. 7c). The baroclinic flux Q_g was largest when the tidal flux Q_{rms} was weakest, as shown in Figs. 7c and 7b, respectively. This indicates that gravitational exchange was important during neap tides when tidal friction was weaker, as indicated by Eq. (23).

Based on the above correlations, we decomposed the subtidal or Eulerian flux from Eq. (11) into its barotropic and baroclinic components:

$$Q_{\mathrm{in}}^{\mathrm{Eu}} = Q_\eta + Q_g, \tag{24}$$

where Q_g is flux due to the estuarine circulation [Eq. (23)] and Q_η is the flux due to subtidal water-level

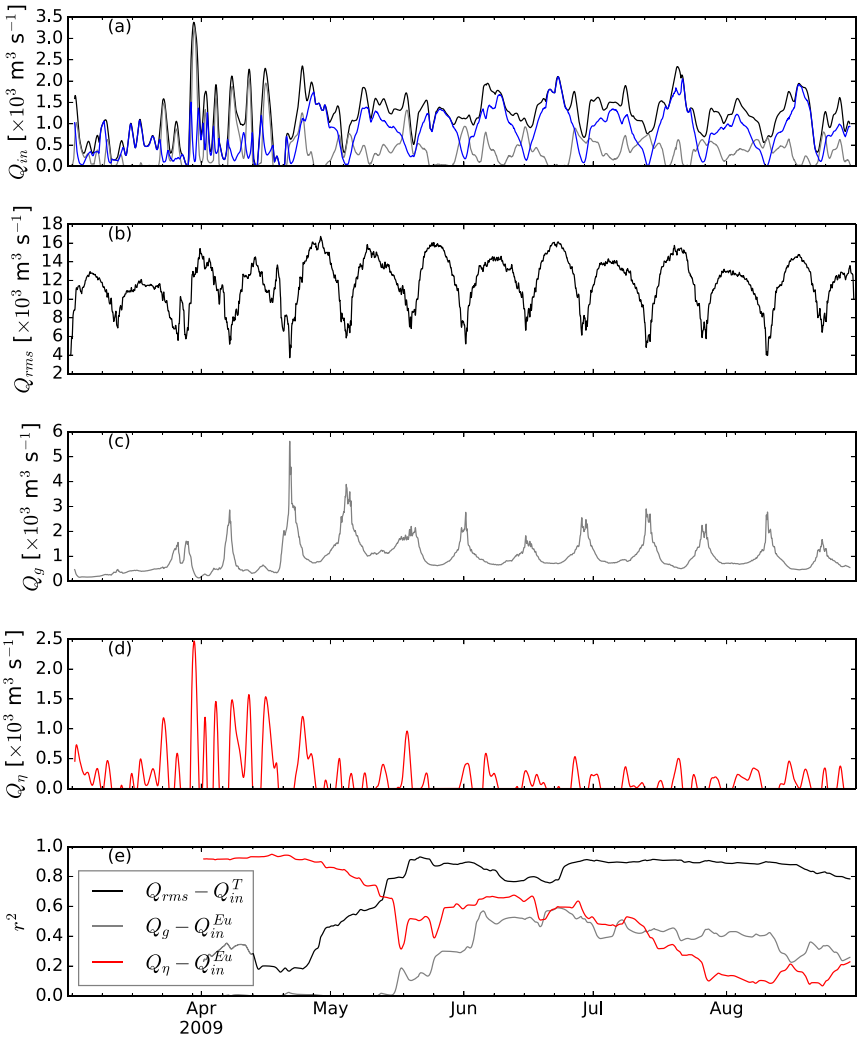

FIG. 7. (a) Decomposed inward isohaline flux components (same as Fig. 5a). (b) RMS tidal flux $Q_{\rm rms}$. (c) Baroclinic exchange flux Q_g. (d) Barotropic velocity flux Q_η. (e) Rolling linear regression between $Q_{\rm in}$ and the quantities in (b)–(d). Rolling regression is for a prior 30-day window and therefore the data start in April.

fluctuations [Eq. (22)]. To calculate Q_g using the box model, we approximated the mean horizontal salinity gradient as

$$\frac{d\langle s\rangle}{dx} = s_o \frac{1-\Sigma}{L_s}, \tag{25}$$

where L_s is the distance along axis to the volumetric mean salinity. For Galveston Bay, L_s is roughly constant and equal to $L/2$ (see Fig. 2a), or more generally, $L_s = L/\text{constant}$, where the constant is determined from the geometry. This will not be the case in many other estuaries, however (e.g., northern San Francisco Bay and the Hudson River), and in these cases $L_s = f(L_x)$. The Eulerian inward exchange flow is then

$$Q_{\rm in}^{\rm Eu} = 2a_g u_* A_{\rm mouth}(1-\Sigma){\rm Si} + a_\eta A_{\rm bay}\frac{d\langle\eta\rangle}{dt}, \tag{26}$$

where

$${\rm Si} = \frac{g\beta s_o H^2}{L u_*^2} \tag{27}$$

TABLE 1. Regression r^2 of each exchange flux component against the barotropic, baroclinic, and tidal flux estimates.

	$Q_{\rm in}$	$Q_{\rm in}^T$	$Q_{\rm in}^{\rm Eu}$
Q_η	0.25	0.03	0.71
Q_g	0.02	0.11	0.04
$Q_{\rm rms}$	0.27	0.66	0.09

is the Simpson number (Geyer and MacCready 2014), which is also referred to as the horizontal Richardson number (Monismith et al. 1996); this captures the relative influence of the horizontal buoyancy gradient against vertical mixing due to tidal friction. Finally, the tidal component of the inward total exchange flow is estimated by

$$Q_{\text{in}}^{T} = a_T Q_{\text{rms}}, \tag{28}$$

where α_T is an empirical coefficient.

Least squares fit of the Galveston Bay SUNTANS numerical model data to Eqs. (26) and (28) resulted in the values of the empirical weights $a_g = 0.22$ and $a_\eta = 0.46$ ($r^2 = 0.71$, RMSE $= 196.0\,\text{m}^3\,\text{s}^{-1}$), and $a_T = 0.15$ ($r^2 = 0.78$, RMSE $= 311.5\,\text{m}^3\,\text{s}^{-1}$). The RMSE of the empirically fit Q_{in} with all three components was $381\,\text{m}^3\,\text{s}^{-1}$ ($r^2 = 0.88$) or roughly ±20%. These results suggest that the inward total exchange flow can be predicted based on the tidal flux, the subtidal water-level fluctuations, and the normalized volume-averaged salinity (Q_{rms}, $\langle\eta\rangle$, and Σ). Furthermore, since the coefficients are $\sim O(1)$, the estimates are also justified from a physical point of view. Quantities Q_{rms} and $\langle\eta\rangle$ are typically measured in major estuaries (e.g., by NOAA PORTS), although estimating Σ from observations is more difficult because of the need for adequate spatial salinity sampling. A simple model for Σ, like Eq. (14), is therefore desirable.

5. Application of the unsteady box model to Galveston Bay

a. Sensitivity testing

Given our model of $\delta(\Sigma)$ [Eq. (21)], and estimates of Q_{in}, we can now solve the box model in Eq. (14) numerically using

$$\Sigma_{n+1} = \Sigma_n + \Delta t\left[\frac{Q_{in,n}}{V}\delta_n - \frac{Q_{r,n}}{V}(1-\delta_n) + \frac{1-(\delta_n+\Sigma_n)}{V}\left.\frac{dV}{dt}\right|_n\right], \tag{29}$$

where subscript n denotes a discrete time value, and δ_n is given at each time step by Eq. (21).

We tested several variations of the box model [Eq. (14)] against the 6-month SUNTANS solution to determine how the unknowns, Q_{in} and δ, affected the prediction. First, we tested two variations of the functional form of δ, namely, constant, and nonlinearly proportional to Σ [i.e., Eq. (21); Fig. 6]. We used the temporal mean $\delta = 0.17$ from the six-month numerical simulation for the constant-δ scenario. These scenarios used a time-dependent inward exchange and volume fluctuations from the numerical model (Fig. 5a). A scenario with $dV/dt = 0$, that is, ignoring the last term in Eq. (14), was also tested. Last, a scenario with constant $Q_{\text{in}} = 1400\,\text{m}^3\,\text{s}^{-1}$ and $dV/dt = 0$, yet still using the nonlinear δ model, was tested.

Results of the different scenarios and the forcing terms are shown in Fig. 8. Qualitatively, all scenarios captured the lagged drop in mean salinity relative to the river flow, followed by a gradual salinity increase over several months. The constant δ scenario performed the worst with an RMSE against the SUNTANS data of 0.088. The nonlinear form of δ resulted in a better prediction with an RMSE = 0.036, indicating the importance of the dependence of δ on the estuarine state. Setting constant Q_{in} resulted in RMSE = 0.032 and therefore a better prediction than setting constant δ. Neglecting the dV/dt term made little difference to the prediction (RMSE = 0.036).

These results show that for Galveston Bay, the low value of δ limits the role of Q_{in} on salinity adjustment. Furthermore, variations in Q_{in} due to changes in tidal forcing, for example, had little overall influence on the salt content because the time scale of the variations were much shorter than the estuarine adjustment time (40–140 days). Likewise, variations in the subtidal volume, which often exceeded the volume inputs from the TEF and river flow (see Fig. 8b), had little effect in Galveston Bay.

b. Long-term salinity prediction using the box model

We now use the box model to predict the mean salt content in Galveston Bay for a longer time period than that covered by the numerical model to show that the box model has utility when a numerical model is not available or is computationally expensive. (The numerical model took roughly 2 weeks to hindcast a 6-month period using 62 CPUs.) To validate the box model, we first developed a 5-yr estimate for the mean salinity using a weighted average of three Texas Water Development Board (TWDB) water-quality monitoring stations: trin, midg, and boli (see Fig. 1 for their locations). We then used the 6-month SUNTANS dataset to fit, via least squares, weights to the model-station data at each of these locations to the modeled mean salinity. The resulting weights for each station were roughly one-third and were assumed time-invariant. A weighted average was then applied to the observations to reconstruct the mean salinity for 5 years. This process of using sparse measurements to estimate the mean salinity resulted in a time series, with some gaps, for the mean salinity from 2007 to 2012.

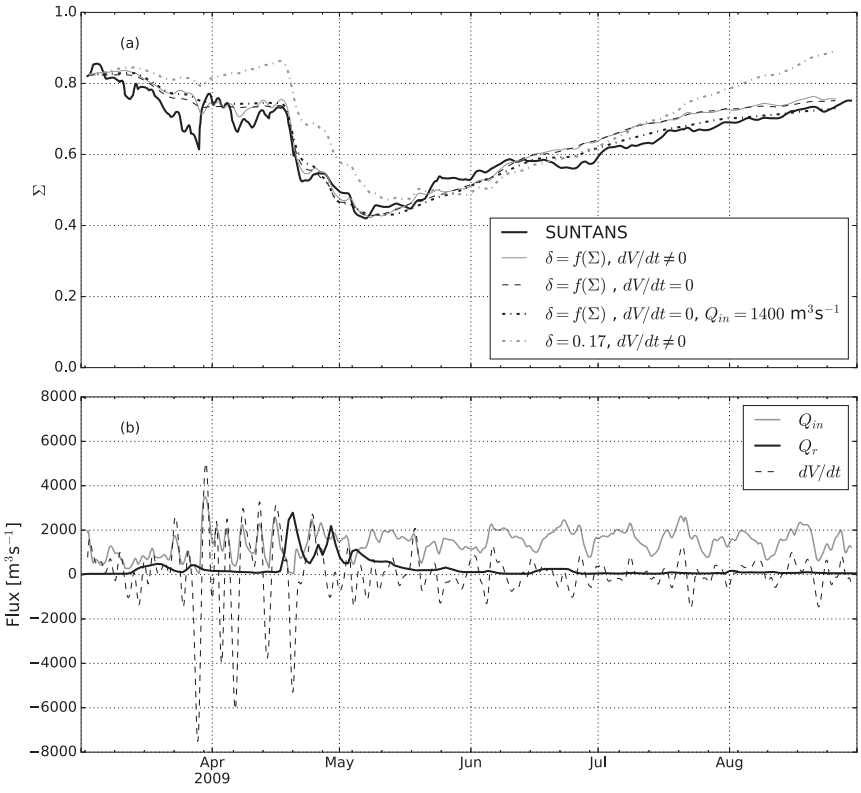

FIG. 8. (a) Normalized volume-averaged salinity Σ using SUNTANS and solutions to variations of Eq. (14). (b) River, TEF, and barotropic fluxes at the mouth of Galveston Bay used to drive the solutions in (a).

The inputs to the box model were the time-variable river discharge, sourced from the TWDB hydrological model (see Rayson et al. 2015), and estimates for the constant volume ($V = 3.75 \times 10^9$ m^3), ocean salinity ($s_{\text{in}} =$ 34 psu), and the inward TEF ($Q_{\text{in}} = 1400\,\text{m}^3\,\text{s}^{-1}$). The time-rate of change of volume dV/dt was calculated from water-level observations [cf. Eq. (22)] collected at Galveston Pier 21 by NOAA (NOAA Station ID: 8771450). We showed in the 6-month hindcast that this particular estuary was insensitive to a time-variable discharge, although Q_{in} could be estimated based on the empirical relationships presented in Eqs. (26) and (28).

Figure 9 shows the best estimate of the mean normalized salinity from the observations, along with the numerical box model [Eq. (29)] solutions, both with and without the dV/dt term. The box model performed well ($r^2 = 0.86$, RMSE = 0.12) and captured both the rapid drop in Σ after each of the large discharge events and the relatively slow salinity adjustment period that followed each event. The model also captured the gradual increase in salt content from mid-2010 to 2012 when there was a drought and in which no discharge events exceeded $500\,\text{m}^3\,\text{s}^{-1}$. Despite the long period of relatively little river forcing, the salinity never reached equilibrium. Note that the inclusion of the dV/dt term made negligible difference to the 5-yr prediction.

The adjustment time, calculated from the box-model solution using Eq. (19) and shown in Fig. 9b, varied by several orders of magnitude (10–1000 days), with the majority of values between 40 and 200 days (Fig. 9c). Adjustment times greater than 1000 days arose during salinity maxima and minima as $d\Sigma/dt \rightarrow 0$. The adjustment time from Eq. (1), which assumes the response is due to a small change in forcing, tended toward the lower bound of the adjustment time from Eq. (19): it predicts the estuary will respond too rapidly. In many estuaries, the river discharge varies by several orders of magnitude, as is the case for Galveston, so the underlying assumptions of Eq. (1) are likely to be violated.

6. Discussion

a. *Mean salinity response to time-dependent river and exchange flow*

Various authors have established a relationship between the salt intrusion length, instead of the mean salt content, and the river discharge (e.g., Monismith et al. 2002). Based on classical estuarine circulation theory

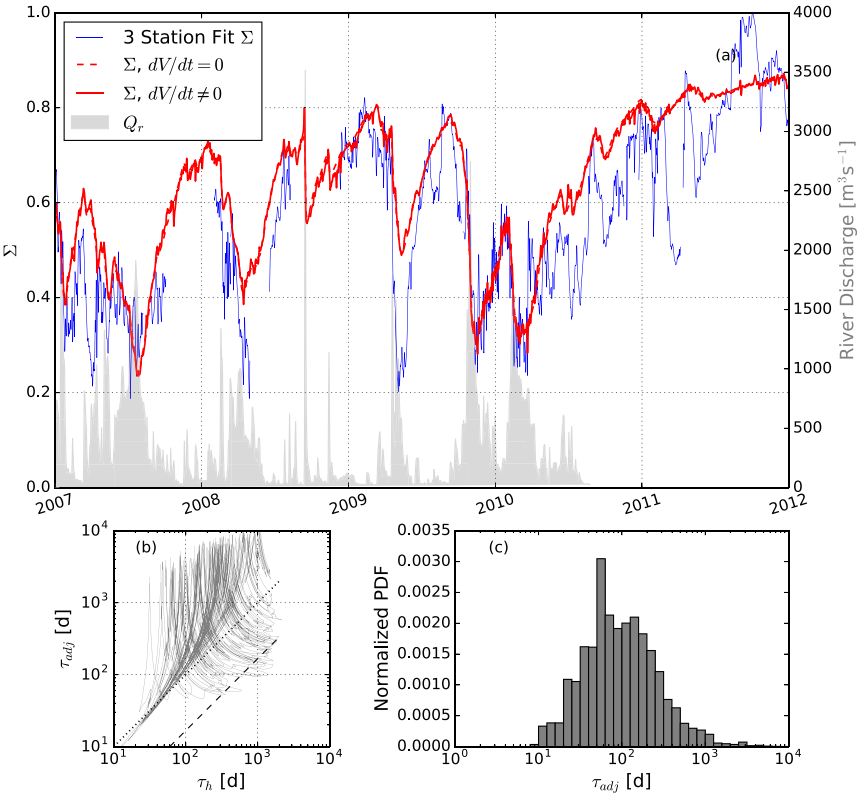

FIG. 9. (a) Five-year normalized salinity prediction, with the normalized salinity difference δ, the best-estimate salinity from field measurements, and the river discharge. Note that the river discharge has a different scale. (b) The adjustment time from Eq. (18) from the 5-yr prediction plotted against the hydraulic flushing time. (c) A histogram of the adjustment time in (b). The black dotted line in (b) is where the adjustment time is equal to the hydraulic flushing time and the dashed line is equal to Eq. (1).

(see, e.g., MacCready and Geyer 2010, and references therein), $L_2 \sim Q_r^{-1/3}$, although Monismith et al. (2002) found that $L_2 \sim Q_r^{-1/7}$ in northern San Francisco Bay. The weaker dependence arises because of bathymetric variability or the effects of stratification on vertical mixing. Bulk salinity quantities, such as the volume-averaged salinity $\overline{\overline{s}} = V^{-1}\int s\,dV$ shown in Fig. 2b (the mean salinity), exhibited a lagged response to river flow, indicating that a power-law relationship is not appropriate for predicting salinity in unsteady estuaries. This point is highlighted in Fig. 10 where the volume-averaged salinity, along with the bulk freshwater fraction f, where (cf. Fischer et al. 1979)

$$f = \frac{1}{V}\int \frac{s_o - s}{s_o}\,dV, \tag{30}$$

and the 5-psu isohaline intrusion length L_5 are plotted against instantaneous river discharge. Hysteresis was evident with all three quantities, indicating that the time history of river flow was important, not just the instantaneous quantity. The location of the 5-psu isohaline L_5 (shown in Fig. 10c) decreased rapidly from 60 to 40 km following the large flooding events in late April 2009 (Fig. 2a). It reached a minimum in early May when Q_r dropped below $1000\,\mathrm{m^3\,s^{-1}}$ and steadily increased back to 60 km by the start of August. The curves indicating different power-law relationships between L_5 and Q_r are also shown in Fig. 10c for reference.

Hilton et al. (1998) showed that the freshwater fraction could be predicted in an estuary with time-dependent river discharge by replacing $Q_r(t)$ with an effective (steady) flow rate $\langle Q_{r,\mathrm{eff}}\rangle$. Assuming a constant residence time allows $\langle Q_{r,\mathrm{eff}}\rangle$ to be computed using a weighted exponential filter on a discrete time series,

$$\left\langle Q_{r,\mathrm{eff}}\right\rangle = \left[1 - \exp\left(\frac{-\Delta t}{\tau}\right)\right]\sum_{n=0}^{\infty} Q_r(t - n\Delta t)\exp\left(\frac{-n\Delta t}{\tau}\right). \tag{31}$$

Based on time scales calculated using various methods in Rayson et al. (2016), we set $\tau = 30$ days and showed

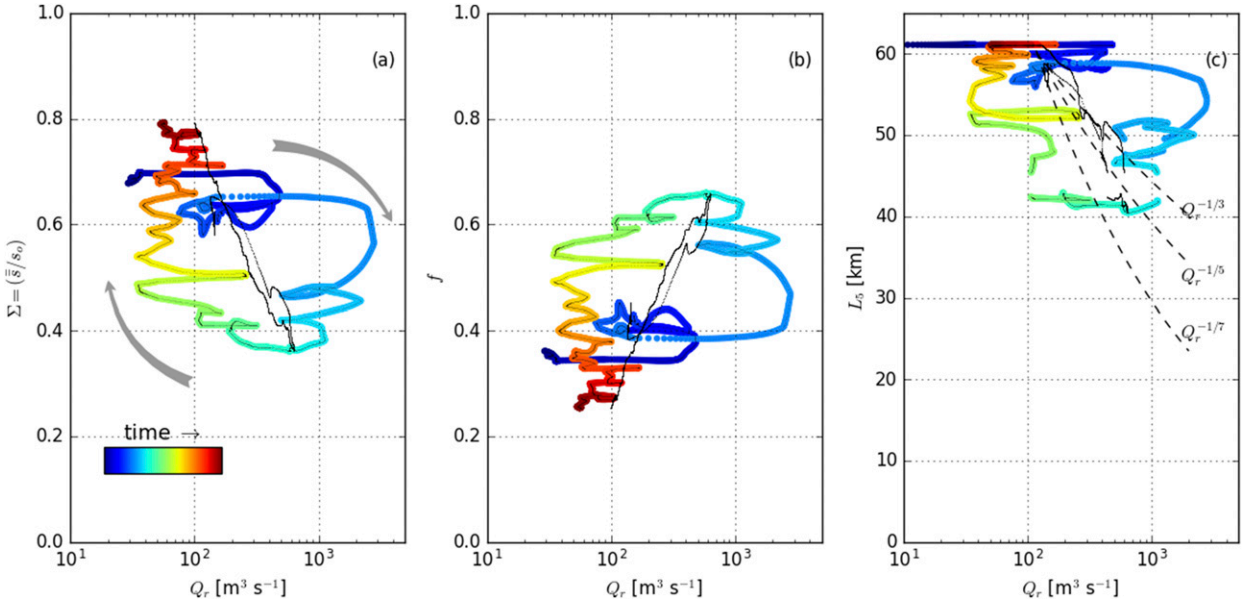

FIG. 10. Scatterplot of the (a) normalized volume-averaged salinity, (b) freshwater fraction, and (c) 5-psu isohaline position L_5 plotted against river discharge. Points are colored by time, and gray arrows indicate the direction in time to highlight the hysteresis. The small black dots in each panel represent the exponentially filtered quantity [Eq. (31)]. Steady-state power-law relationships are shown in (c) for comparison.

the relationships between $\langle Q_{r,\text{eff}} \rangle$ and Σ, f, and L_5 in Figs. 10a–c, respectively. Filtering shows that results collapse onto lines of the form $\langle Q_{r,\text{eff}} \rangle^{-n}$. The main assumption of Eq. (31) is that the filter time scale τ is constant. Rayson et al. (2016) demonstrated that various estuarine time scales in Galveston Bay are not constant, but are actually weakly dependent on river flow history. We found that $\Sigma \sim \langle Q_{r,\text{eff}} \rangle^{-1/2.5}$, although the exponent value was sensitive to the filter time scale. The best-fit value of the power, n in $L_5 \sim \langle Q_{r,\text{eff}} \rangle^{-1/n}$, was $n \approx 5.0$, as shown in Figs. 10a–c. Predicting Σ (or L_5) using a power-law relationship is problematic for unsteady systems because it relies on a constant time-scale assumption. As demonstrated in Fig. 9, a time-dependent box model more suitably captures the salinity response in an unsteady estuary like Galveston Bay.

b. *Adjustment time*

As stated in the introduction, the adjustment time is important because it can be used to determine whether an estuary is steady, quasi steady, or unsteady. The adjustment time in Galveston Bay is $\sim O$(10–100) days, and the forcing time scales are about 14 days for tides and $\sim O$(10) days for high river flow events. Since the adjustment time is greater than the forcing time scales, Galveston Bay is an unsteady estuary.

The salinity adjustment time is ultimately dependent on the ocean water replacement time $V/[\delta Q_{\text{in}}]$ and the freshwater replacement time $V/[(1-\delta)Q_r]$. The low value of δ (<0.25) implies that Galveston Bay is more responsive to changes in freshwater flow and less responsive to variations in Q_{in}. For an average $\delta = 0.2$, Q_{in} must be 4 times greater than Q_r for the salinity to increase. In general, low δ in any estuary implies that salt intrusion adjustment is relatively slow during low-discharge periods, which will be the case in any partially or well-mixed systems.

The estuarine speedup factor from Eq. (20) is shown in Fig. 11 when $\Sigma = 0.3$ and 0.7 (the approximate range from the Galveston Bay numerical dataset). Figure 11 illustrates how the estuarine speedup factor is greater for lower salinity, meaning a low-salinity estuary will respond faster than the freshwater replacement time. For Galveston Bay, τ_{adj} from Eq. (18) was, on average, 40 days during the high river discharge period (17 April–10 May 2009) and 140 days during the low discharge period (11 May–30 September 2009). Although the estuarine speedup factor was $\sim O(10)$ during low flow conditions ($\delta = 0.3$, $Q_{\text{in}}/Q_r > 10$), the total adjustment time was lower because of the lower total discharge.

Figure 11 shows the estuarine speedup factor from Eq. (20) in the same parameter space as Hansen and Rattray (1966)'s "ν diagram" (their Fig. 1). Note that here Q_{in} has a different meaning than their u_s. The region of this parameter space occupied by the Hudson River and Puget Sound was sourced from studies by Chen et al. (2012) and Sutherland et al. (2011), respectively, who also used the TEF technique. Both

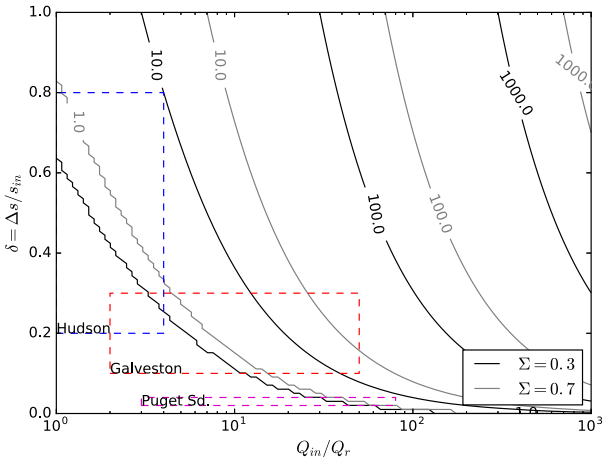

FIG. 11. Estuarine speedup factor τ^* in $(Q_{in}/Q_r) - (\Delta s/s_{in})$ parameter space [Eq. (20)]. The black and gray contours are for $\Sigma = 0.3$ and $\Sigma = 0.7$, respectively (Galveston Bay and Puget Sound). Estimates for the Hudson River and Puget Sound parameters were derived from Chen et al. (2012) and Sutherland et al. (2011), respectively.

estuaries occupy different regions of this parameter space than Galveston Bay. Figure 11 shows that the speedup factor for the Hudson River, for example, is 10 and 5 when Σ is 0.3 and 0.7, respectively, for $Q_{in}/Q_r = 4$ and $\delta = 0.8$. It means that the speedup factor will be twice as fast when the estuary contains less salt (shorter salt intrusion length). In contrast, the speedup factor in a much larger system like Puget Sound will be less asymmetric, except when the exchange flow–to–river flow ratio is $\sim O(100)$. For $Q_{in}/Q_r = 1$–50 and $\delta = 0.05$, the speedup factor is constant for Puget Sound. Galveston Bay covers the region of this parameter space with greater speedup factor but also has an asymmetric speedup factor depending on the initial mean salinity. For $Q_{in}/Q_r = 60$ and $\delta = 0.25$, the speedup factor is roughly 50 and 20 for $\Sigma = 0.3$ and 0.7, respectively. Figure 11 highlights that the speedup factor will be greater for all of these estuaries with a lower initial salt content.

The sensitivity of δ to Σ predicts the relative influence of Q_{in} and Q_r on the adjustment time for a particular estuary. Substituting Eq. (21) into Eq. (19) results in

$$\tau_{adj} = \frac{V\Sigma}{(1-\Sigma)^2(Q_{in}+Q_r) - Q_r}, \tag{32}$$

which shows that $\tau_{adj} \propto \Sigma(1-\Sigma)^{-2}$, that is, longer adjustment time for higher Σ. Chen (2015) showed that the nonlinear relationship between the exchange flux and salt intrusion length caused an asymmetric adjustment time during rising and falling river discharge rates in an idealized Hudson River. His scaling assumes that gravitational circulation is the main driver of exchange flow so that $F_{in} \propto L_x^{-3}$. Equation (32) predicts asymmetric adjustment times based on the initial salinity. It makes no assumption about exchange flow scaling, although a nonlinear relationship between the adjustment time and the mean salinity arises because of the relationship between the stratification at the mouth and the mean salinity [Eq. (21)]. A property of the $\delta - \Sigma$ relationship in Eq. (21) is that the slope $d\Sigma/d\delta \to 0$ as $\Sigma \to 1$, suggesting weak dependence on δ when there is high salinity, whereas $d\Sigma/d\delta \to \infty$ as $\Sigma \to 0$, suggesting strong dependence on δ when there is low salinity.

7. Conclusions

We have used the Q_{in} and Δs values calculated using an isohaline flux analysis of a realistic 3D hydrodynamic model of Galveston Bay to drive an unsteady box model. The primary objective of using this simple model was to show that TEF terms can be used to predict the mean salinity with unsteady forcing. A second objective was to use the model to conceptually highlight how different estuaries will respond based on these variables. The ultimate goal was to build an analysis tool capable of attributing the mean estuarine salinity response to changes in variables that are usually measured, such as the volume V, river flow Q_r, and ocean salinity s_{in}. We used a 3D numerical solution to establish the range of the inward exchange flow Q_{in}, the other necessary component of the model. However, as shown in section 4, Q_{in} can be parameterized based on the tidal forcing, the low-frequency water-level fluctuations, and the longitudinal salinity gradient. These parameterizations can then be used to predict the salt content much more efficiently over a longer time period (see Fig. 9).

Galveston Bay, like many other Gulf of Mexico estuaries, is characterized by a narrow entrance with a wide, shallow, geometrically complex interior. Freshwater discharge is highly time dependent and comes from multiple locations. It is often incorrectly assumed that these estuaries are vertically well mixed and that flushing is driven solely by tidal motions (e.g., Officer 1976). We have shown, through the TEF analysis, that salt exchange is due to a combination of tidal, low-frequency barotropic forcing and steady exchange flow and that their relative contributions vary with both time and distance from the estuary mouth. All of these complexities make it difficult to apply existing models for predicting salt intrusion length, or, more generally, volume-averaged salt content.

Posing the estuarine adjustment problem in terms of a simple box model, as we have done here, helps elucidate the time-dependency effects in different estuaries and

reduces the aforementioned complexities of the problem. Using scaling arguments to predict salt content (or intrusion length) and salt difference at the mouth from instantaneous river flow, that is, L_x (or Σ) $\sim Q_r^{-1/n}$, requires time-averaging the inputs in order to satisfy a steady-state assumption and apply existing theory (e.g., Geyer 2010; Guha and Lawrence 2013). Unambiguously defining this averaging time scale is an issue because, as we have shown here and as was also shown in Rayson et al. (2016), estuarine transport time scales are themselves time dependent. The box model used here bypasses this issue of time-averaging the forcing and captures the relationships between river flow, exchange flow, and the mean salt content.

One aspect of the box model that will vary between different estuaries is the relationship between the normalized difference between inflow and outflow salinity at the mouth δ and the normalized salt content Σ. Using a steady-state assumption, Geyer (2010) showed that the normalized salinity difference can be modeled with a freshwater Froude number [Eq. (15)]. Here, we have simplified Guha and Lawrence (2013) and shown that for Galveston Bay, the normalized salinity difference is proportional to the horizontal salinity gradient squared [Eq. (21); Fig. 6]. This simplification has the practical advantage of not requiring an estuarine Froude number that will have an ambiguous definition in a topographically complex estuary with highly variable river forcing. Our $\delta - \Sigma$ model in Eq. (21) is appropriate in other estuaries with a linear salinity gradient and $\mathrm{Fr}_f \approx 0.05$; otherwise, the original Guha and Lawrence (2013) formulation [Eq. (17)] is likely to be more suitable for estuaries with larger Fr_f. As pointed out by Guha and Lawrence (2013), the normalized salinity difference dependence on the longitudinal salinity gradient can only be ignored when $\mathrm{Fr}_f \ll 1$. The important contribution here is the inclusion of the longitudinal salinity gradient in the normalized salinity difference model.

The other unknown in the box model is the inward total exchange flow Q_{in}. Chen et al. (2012) showed that Q_{in} scales with the tidal flux for short estuaries (defined as when the ratio of tidal excursion distance to estuary length is large) and that a Simpson number scaling is more appropriate for long estuaries. We showed that at the mouth of Galveston Bay, Q_{in} scales linearly with both the tidal flux and the Simpson number even though this estuary would be classified as long based on this definition. Finally, since the adjustment time in Galveston Bay is long relative to the time scale of change in total exchange flow, which is mainly due to fortnightly tidal modulations, a constant time-averaged Q_{in} was suitable to predict mean salinity for a 5-yr period. In estuaries where the adjustment time is closer to the forcing time scale, a time-dependent total exchange flow will be necessary. Empirical estimates of the total exchange flow based on tidal forcing and/or the Simpson number are, however, possible to obtain, given suitable numerical model or observation data.

Acknowledgments. This work was supported by a grant from the Gulf of Mexico Research Initiative (GOMRI) as part of the Gulf Integrated Spill Response (GISR) Consortium. Model data are archived at the Gulf of Mexico Research Initiative Information and Data Cooperative (https://data.gulfresearchintiative.org) as dataset R1.x137.000:0017 (doi:10.7266/N77H1H0B). We thank three anonymous reviewers for their useful comments that improved earlier versions of this manuscript.

REFERENCES

Banas, N., B. Hickey, P. MacCready, and J. Newton, 2004: Dynamics of Willapa Bay, Washington: A highly unsteady, partially mixed estuary. *J. Phys. Oceanogr.*, **34**, 2413–2427, https://doi.org/10.1175/JPO2637.1.

Chen, S.-N., 2015: Asymmetric estuarine responses to changes in river forcing: A consequence of nonlinear salt flux. *J. Phys. Oceanogr.*, **45**, 2836–2847, https://doi.org/10.1175/JPO-D-15-0085.1.

——, W. Geyer, D. Ralston, and J. Lerczak, 2012: Estuarine exchange flow quantified with isohaline coordinates: Contrasting long and short estuaries. *J. Phys. Oceanogr.*, **42**, 748–763, https://doi.org/10.1175/JPO-D-11-086.1.

Dronkers, J., and J. van de Kreeke, 1986: Experimental determination of salt intrusion mechanisms in the Volkerak estuary. *Neth. J. Sea Res.*, **20**, 1–19, https://doi.org/10.1016/0077-7579(86)90056-6.

Fischer, H. B., E. J. List, R. C. Y. Koh, J. Imberger, and N. H. Brooks, 1979: *Mixing in Inland and Coastal Waters*. Academic Press, 483 pp.

Fringer, O. B., M. Gerritsen, and R. L. Street, 2006: An unstructured-grid, finite-volume, nonhydrostatic, parallel coastal ocean simulator. *Ocean Modell.*, **14**, 139–173, https://doi.org/10.1016/j.ocemod.2006.03.006.

Geyer, W. R., 2010: Estuarine salinity structure and circulation. *Contemporary Issues in Estuarine Physics*, 1st ed. A. Valle-Levinson, Ed., Cambridge University Press, 12–26.

——, and P. MacCready, 2014: The estuarine circulation. *Annu. Rev. Fluid Mech.*, **46**, 175–197, https://doi.org/10.1146/annurev-fluid-010313-141302.

Guha, A., and G. A. Lawrence, 2013: Estuary classification revisited. *J. Phys. Oceanogr.*, **43**, 1566–1571, https://doi.org/10.1175/JPO-D-12-0129.1.

Hansen, D., and M. Rattray, 1966: New dimensions in estuary classification. *Limnol. Oceanogr.*, **11**, 319–326, https://doi.org/10.4319/lo.1966.11.3.0319.

Hetland, R. D., and W. Geyer, 2004: An idealized study of the structure of long, partially mixed estuaries. *J. Phys. Oceanogr.*, **34**, 2677–2691, https://doi.org/10.1175/JPO2646.1.

Hilton, A. B. C., D. L. McGillivary, and E. E. Adams, 1998: Residence time of freshwater in Boston's inner harbor. *J. Waterw. Port Coastal Ocean Eng.*, **124**, 82–89, https://doi.org/10.1061/(ASCE)0733-950X(1998)124:2(82).

Jassby, A. D., W. J. Kimmerer, S. G. Monismith, C. Armor, J. E. Cloern, T. M. Powell, J. R. Schubel, and T. J. Vendlinski, 1995: Isohaline position as a habitat indicator for estuarine populations. *Ecol. Appl.*, **5**, 272–289, https://doi.org/10.2307/1942069.

Knudsen, M., 1900: Ein hydrographischer lehrsatz. *Ann. Hydrogr. Marit. Meteor.*, **28**, 316–320.

Kranenburg, C., 1986: A time scale for long-term salt intrusion in well-mixed estuaries. *J. Phys. Oceanogr.*, **16**, 1329–133, https://doi.org/10.1175/1520-0485(1986)016<1329:ATSFLT>2.0.CO;2.

Largier, J. A., 2010: Low-inflow estuaries: Hypersaline, inverse and thermal scenario. *Contemporary Issues in Estuarine Physics*, 1st ed. A. Valle-Levinson, Ed., Cambridge University Press, 247–272.

Lerczak, J. A., and W. R. Geyer, 2004: Modeling the lateral circulation in straight, stratified estuaries. *J. Phys. Oceanogr.*, **34**, 1410–1428, https://doi.org/10.1175/1520-0485(2004)034<1410:MTLCIS>2.0.CO;2.

——, ——, and D. K. Ralston, 2009: The temporal response of the length of a partially stratified estuary to changes in river flow and tidal amplitude. *J. Phys. Oceanogr.*, **39**, 915–933, https://doi.org/10.1175/2008JPO3933.1.

MacCready, P., 1999: Estuarine adjustment to changes in river flow and tidal mixing. *J. Phys. Oceanogr.*, **29**, 708–726, https://doi.org/10.1175/1520-0485(1999)029<0708:EATCIR>2.0.CO;2.

——, 2004: Toward a unified theory of tidally-averaged estuarine salinity structure. *Estuaries*, **27**, 561–570, https://doi.org/10.1007/BF02907644.

——, 2007: Estuarine adjustment. *J. Phys. Oceanogr.*, **37**, 2133–2145, https://doi.org/10.1175/JPO3082.1.

——, 2011: Calculating estuarine exchange flow using isohaline coordinates. *J. Phys. Oceanogr.*, **41**, 1116–1124, https://doi.org/10.1175/2011JPO4517.1.

——, and W. R. Geyer, 2010: Advances in estuarine physics. *Annu. Rev. Mar. Sci.*, **2**, 35–58, https://doi.org/10.1146/annurev-marine-120308-081015.

Marta-Almeida, M., R. D. Hetland, and X. Zhang, 2013: Evaluation of model nesting performance on the Texas–Louisiana continental shelf. *J. Geophys. Res. Oceans*, **118**, 2476–2491, https://doi.org/10.1002/jgrc.20163.

Monismith, S. G., 2017: An integral model of unsteady salinity intrusion in estuaries. *J. Hydraul. Res.*, **55**, 392–408, https://doi.org/10.1080/00221686.2016.1274682.

——, J. Burau, and M. Stacey, 1996: Stratification dynamics and gravitational circulation in northern San Francisco Bay. *San Francisco Bay: The Ecosystem*, J. T. Hollibaugh, Ed., American Association for the Advancement of Science Pacific Division, 123–153.

——, W. Kimmerer, J. R. Burau, and M. T. Stacey, 2002: Structure and flow-induced variability of the subtidal salinity field in northern San Francisco Bay. *J. Phys. Oceanogr.*, **32**, 3003–3019, https://doi.org/10.1175/1520-0485(2002)032<3003:SAFIVO>2.0.CO;2.

Officer, C. B., 1976: *Physical Oceanography of Estuaries (and Associated Coastal Waters)*. John Wiley and Sons, 480 pp.

Orlando, S. P., L. P. Rozas, G. H. Ward, and C. J. Klein, 1993: Salinity characteristics of Gulf of Mexico estuaries. NOAA Office of Ocean Resources Conservation and Assessment Tech. Rep., 209 pp., https://docs.lib.noaa.gov/noaa_documents/NOS/ORCA/National_Esturarine_Inventory/Gulf_of_Mexico_1993.pdf.

Powell, E. N., J. M. Klinck, E. E. Hofmann, and M. A. McManus, 2003: Influence of water allocation and freshwater inflow on oyster production: A hydrodynamic–oyster population model for Galveston Bay, Texas, USA. *Environ. Manage.*, **31**, 100–121, https://doi.org/10.1007/s00267-002-2695-6.

Ralston, D. K., W. R. Geyer, and J. A. Lerczak, 2008: Subtidal salinity and velocity in the Hudson River estuary: Observations and modeling. *J. Phys. Oceanogr.*, **38**, 753–770, https://doi.org/10.1175/2007JPO3808.1.

Rayson, M. D., E. S. Gross, and O. B. Fringer, 2015: Modeling the tidal and sub-tidal hydrodynamics in a shallow, micro-tidal estuary. *Ocean Modell.*, **89**, 29–44, https://doi.org/10.1016/j.ocemod.2015.02.002.

——, ——, R. D. Hetland, and O. B. Fringer, 2016: Time scales in Galveston Bay: An unsteady estuary. *J. Geophys. Res. Oceans*, **121**, 2268–2285, https://doi.org/10.1002/2015JC011181.

Simpson, J., J. Brown, J. Matthews, and G. Allen, 1990: Tidal straining, density currents, and stirring in the control of estuarine stratification. *Estuaries*, **13**, 125–132, https://doi.org/10.2307/1351581.

Stacey, M., J. R. Burau, and S. G. Monismith, 2001: Creation of residual flows in a partially stratified estuary. *J. Geophys. Res.*, **106**, 17 013–17 037, https://doi.org/10.1029/2000JC000576.

Sutherland, D. A., P. MacCready, N. S. Banas, and L. F. Smedstad, 2011: A model study of the Salish Sea estuarine circulation. *J. Phys. Oceanogr.*, **41**, 1125–1143, https://doi.org/10.1175/2011JPO4540.1.

Wong, K.-C., and J. E. Moses-Hall, 1998: On the relative importance of the remote and local wind effects to the subtidal variability in a coastal plain estuary. *J. Geophys. Res.*, **103**, 18 393–18 404, https://doi.org/10.1029/98JC01476.